PCCP

PAPER

View Article Online
View Journal | View Issue

Cite this: *Phys. Chem. Chem. Phys.*, 2025, **27**, 14240

High resolution infrared spectroscopy of monodeutero-oxirane (*c*-C_2H_3DO) and analysis of two fundamentals between 820 and 950 cm^{-1}†

Sieghard Albert,[a] Ziqiu Chen,[ab] Karen Keppler,[a] Gunther Wichmann,[a] Martin Quack,*[a] Jürgen Stohner,[c] Volker Schurig[d] and Oliver Trapp[e]

Received 5th March 2025,
Accepted 26th April 2025

DOI: 10.1039/d5cp00880h

rsc.li/pccp

We report the analysis of the infrared (IR) spectrum of monodeutero-oxirane (*c*-CH_2CHDO), measured at room temperature at a self-apodized instrumental resolution of 0.0015 cm^{-1} with the Bruker IFS 125 HR Zürich Prototype spectrometer (ZP 2001), in the range of the ring deformation fundamental ν_{12} centered at 896.025 cm^{-1} and the wagging fundamental ν_{13} centered at 837.36 cm^{-1}. A total of more than 1100 transitions were analyzed and fitted with an effective Hamiltonian which represents the data accurately, within 0.001 cm^{-1} for ν_{12} and 0.004 cm^{-1} for most transitions of ν_{13}. We also report *ab initio* calculations including parity violation and an extended analysis with a substantial number of further assigned lines in our previously measured pure rotational spectra in the GHz and far infrared range. In combination with ground state combination differences from the IR spectra and further available results, we provide a critical analysis and improved spectroscopic parameters for the vibrational ground state based on more than 3300 assigned rotational transitions. The results are discussed as they pertain to isotopic chirality, molecular parity violation and the astrophysical observation of this isotopomer.

1 Introduction

The concept of isotopic chirality is of fundamental interest because it introduces a completely new isotope effect arising from the parity violating weak nuclear force.[1–5] Because of the different weak charge of isotopes with different numbers of neutrons, the enantiomers of molecules which become chiral by isotopic substitution are predicted to have different ground state energies, separated by a parity violating energy difference $\Delta_{pv}E$, which can in principle be measured in special experiments,[6] although no successful experiment has been reported to date despite ongoing efforts reviewed previously.[4] $\Delta_{pv}E$ would be exactly zero by symmetry for the symmetric "parent" molecule.

Isotopic chirality also has possible astrophysical implications. In this context we have initiated, some time ago, a project to provide high resolution spectroscopic analyses for chiral isotopomers of the achiral cyclic molecule oxirane, $^{12}C_2H_4{}^{16}O$, which had been detected by astrophysical spectroscopy starting already in 1997[7] followed by several further observations.[8–11] Oxirane might also be the carrier of some of the unidentified infrared bands in astrophysical spectroscopy.[12,13]

Oxirane has a total of four achiral deutero isotopomers C_2H_4O, C_2D_4O, CH_2CD_2O, and *cis*-CHDCHDO. It also has a total of 6 chiral isotopomers, R-C_2H_3DO, S-C_2H_3DO, R-C_2HD_3O, R-C_2HD_3O, R-*trans*-CHDCHDO, and S-*trans*-CHDCHDO. We have previously reported the analyses of high-resolution rotational spectra of the isotopomers C_2H_3DO, and *trans*-CHDCHDO which are the most likely ones to be detected by astrophysical spectroscopy.[14,15] In our previous work we suggested explicitly with predictions from our analysis of the rotational spectra for the 300 to 370 GHz range that this molecule might lead to the first detection of an isotopically chiral molecule by astrophysical spectroscopy, because in this range undeuterated oxirane had been detected in the low mass protostar IRAS-2422 using the Atacama Large Millimeter/Submillimeter Array (ALMA).[11,16] Following our predictions, Müller *et al.* were, indeed, very recently able to identify the corresponding lines of *c*-C_2H_3DO towards IRAS 16293-2422B.[17]

With the recent successful launch of the James Webb Space Telescope[18–21] there is a new path toward the astrophysical observation of molecules by infrared spectroscopy. In this

[a] *Department of Chemistry and Applied Biosciences, ETH Zürich, CH-8093 Zürich, Switzerland. E-mail: martin@quack.ch; Web: https://www.ir.ETHz.CH*
[b] *College of Chemistry and Chemical Engineering, Lanzhou University, Lanzhou 730000, China*
[c] *Institute for Chemistry and Biotechnology ICBT, Zürich University of Applied Sciences ZHAW, Campus Reidbach, CH-8820 Wädenswil, Switzerland*
[d] *Institut für Organische Chemie, Universität Tübingen, D-72076 Tübingen, Germany*
[e] *Department of Chemistry, Ludwig Maximilians University, D-80539 Munich, Germany*

† Electronic supplementary information (ESI) available. See DOI: https://doi.org/10.1039/d5cp00880h

context there exists the tantalizing possibility of detecting a very strong signature of extraterrestrial life by means of infrared spectroscopy using vibrational circular dichroism to search for a possible consistent extraterrestrial homochirality as suggested in ref. 22. We therefore have also studied high resolution infrared spectra of C_2H_3DO and report here the results of the corresponding analysis.

Monodeutero-oxirane (*c*-C_2H_3DO or monodeutero-ethylene oxide), shown in Fig. 1, lends itself well to investigation as a simple, isotopically chiral molecule. As mentioned above, the parent species *c*-C_2H_4O has been detected in a variety of interstellar environments.[7–11,23] Also detected have been vinyl alcohol[24] and acetaldehyde,[25] of which *c*-C_2H_4O is a kinetically stable isomer. It has been predicted to exist in the atmosphere of Titan as well,[26] which is particularly interesting because the chemistry of Titan's atmosphere might provide information about the formation of terrestrial prebiotic compounds.[27] It has also been proposed as a carrier for the Unidentified Infrared Bands (UIBs).[12] The molecule and its isotopomers have been the subject of theoretical studies by Puzzarini *et al.*,[28] who have investigated not only the main species *c*-C_2H_4O, but also the singly deuterated isotopomer *c*-C_2H_3DO.

Oxirane and its isotopomers have been the subject of many experimental infrared,[29–35] microwave,[36–38] and submillimeter wave[39] studies. In addition to the older studies, there have been several recent investigations of the spectrum of the undeuterated oxirane, including the work on the ν_{15}, ν_{12}, ν_5, ν_{10} and ν_2 bands in the infrared at high resolution by Flaud *et al.*[29] and Kwabia Tchana *et al.*[40] The ν_3 band at 1270.4 cm^{-1} has been examined by Russell and Wesendrup[35] and by Ngom *et al.*[41] The ν_1 fundamental at 3018.3 cm^{-1} has been studied by W. J. Lafferty *et al.*[42] Undeuterated oxirane has been examined in the ground state by Pan *et al.*[39] and by Medcraft *et al.*[30] There is less information available in the literature thus far about the spectrum of the isotopomers. Experimental investigations in the microwave region were conducted by Hirose[43] and in the infrared at limited resolution by Nakanaga[33,34] more than 40 years ago. The calculated band centers and intensities of infrared bands have been published by Puzzarini *et al.*[28] Müller *et al.* have recently published a study of the doubly deuterated *c*-CD_2CH_2O and its tentative detection toward IRAS 16293-2422B.[17,44]

We had previously reported the analysis of the THz and GHz spectrum of *c*-C_2H_3DO in the vibrational ground state.[14] For that study, the GHz spectrum of *c*-C_2H_3DO was recorded using our GHz setup at the ETH Zürich[45] and the THz spectrum was recorded using our ETH-protoype FTS (Fourier Transform Spectrometer) at the Swiss Light Source (SLS) with a best resolution close to 0.0005 cm^{-1}.[13] In the meantime, we have been able to assign more than 1000 further lines in the THz spectra in the range of 0.75–1.84 THz and have noted that inadvertently in our previous publication, pre-final tables appeared in print, including uncorrected misprints. Also, most recently, Müller *et al.* have provided additional rotational lines in the submm (GHz) range, together with an analysis including our previous data.[17] In order to provide an optimal starting point for our new analysis of the vibrational spectra, we have therefore re-examined the rotational spectra of the ground state, conducting a global analysis of all currently available data including combination differences from the IR-spectra. We have used these new molecular parameters obtained for the ground state to conduct the first rovibrational high-resolution analysis of the mid-infrared spectrum of *c*-C_2H_3DO. We are able to completely resolve the rovibrational structure of the far and mid infrared spectra of substituted oxiranes with our Bruker prototype spectrometer IFS 125 HR (ZP 2001)[46,47] ($\Delta\tilde{\nu}$ = 0.0007 cm^{-1}). Due to the resolution with which it is possible to measure infrared spectra in our laboratory, we can not only nearly fully assign the infrared spectrum in this region but can also characterize interactions between the rovibrational states of *c*-C_2H_3DO, thus providing insight into the structure and dynamics of this molecule.

The bands for which the analysis is presented here, ν_{12} (ring deformation) and ν_{13} (CHD wag), are the strongest absorption bands in this part of the spectrum of the singly deuterated (and singly fluorinated[31]) species. The need of using the sextic constants in the analysis of the ν_{12} transitions when they are fit independently of the ν_{13} transitions indicates that there exists a strong interaction between the ν_{12} and several other nearby states. The interaction has already been reported by Nakanaga[33] in lower resolution studies of the undeuterated and fully deuterated species of oxirane. The existence of a Coriolis-type resonance has also been proposed by Russell and Wesendrup[35] in their high-resolution study of the ν_3 state of the main species. Coriolis resonances have been examined between the ν_2 and ν_{10} states in the spectrum of the undeuterated oxirane by Kwabia Tchana *et al.*[48] as well.

The present publication is organized as follows: in Section 2 we briefly summarize the synthesis of *c*-C_2H_3DO and the FTIR measurements. In Section 3 we provide a short summary of theoretical results including *ab initio* calculations of the harmonic and anharmonic vibrational frequencies and fundamental transitions, as well as some theoretical results on parity violation in this molecule. We also provide a very brief summary of the basic theoretical background and definitions for

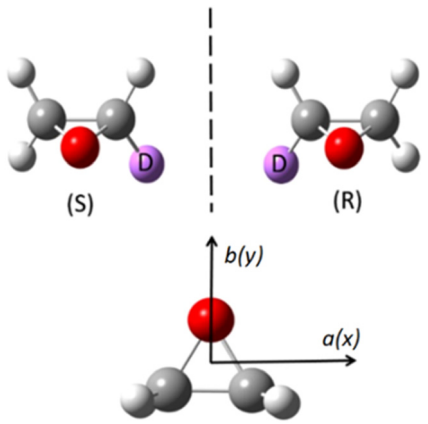

Fig. 1 C_2H_3DO (monodeutero-oxirane): structure and axes. In the lower part the *c*(*z*) axis is perpendicular to the plane pointing towards the observer in a right-handed coordinate system. The *D* atom is hidden behind the plane (here, the axes are shown for the symmetrical C_2H_4O, in C_2H_3DO they are moved away from the symmetrical position).

the effective Hamiltonians used in the analysis of the spectra. In Section 4 we present the new critical analysis of the vibrational ground state. Section 5 describes the assignment of the infrared spectra and the corresponding results of the analysis. In Section 6 we conclude with a discussion of the results and an outlook. Some preliminary results of our work have previously been reported.[49–52]

2 Experimental

2.1 Synthesis

The singly deuterated isotopomer of C_2H_4O was synthesized as a racemate according to the procedure briefly described elsewhere[14] and summarized here in Fig. 2. In a protective atmosphere, vinyl magnesium chloride solution in THF was quenched with deuterium oxide and the monodeuteroethane produced was introduced into a freshly prepared solution of acetylhypobromide (from silver acetate and bromine) in anhydrous tetrachloromethane. After the reaction was completed, the solution was washed with 10% sodium hydrogen sulfate and dried over magnesium sulfate, and the solvent was removed. The crude product (1-acetoxy-2-bromo[2*H*]ethane) was distilled under vacuum (60 °C at 30 torr, yield 80%). 1-Acetoxy-2-bromo[2*H*]ethane and 25% sodium hydroxide in solution were combined in a flask equipped with a condenser filled with a molecular sieve (3 Å) and a nitrogen gas inlet. The flask was heated to 100 °C and monodeutero-oxirane was condensed in a cryogenic trap. The product was redistilled at 10.7 °C (yield 68%). The product was identified by NMR and mass spectrometry and the identity and purity were also obvious from the GHz and THz spectra obtained.[14] Here, as seen in the survey spectrum in the spectral region examined in this work (Fig. 3), carbon tetrachloride CCl_4 and methylene chloride CH_2Cl_2 were present as impurities. However, this did not adversely affect the analysis of the spectrum at high resolution.

2.2 FTIR spectrum

We have recorded the infrared spectrum of monodeutero-oxirane in the region from 600 to 1000 cm^{-1} and beyond, and in particular 800 to 960 cm^{-1} at 295 K at a nominal instrumental resolution of 0.0015 cm^{-1} given by $0.9/d_{MOPD}$ (Maximum Optical Path Difference),[47] slightly less than the Doppler width of C_2H_3DO spectra in this region at room temperature ($\Delta\tilde{\nu}_D$ = 0.0018 cm^{-1}). An absorbance path length l = 18 cm in a glass cell equipped with KBr windows and several sample pressures were chosen (aperture 1.3 mm, spectrum self-apodized). The spectrum used for this analysis was measured with a pressure of 1.8 mbar, the partial pressure of C_2H_3DO being uncertain,

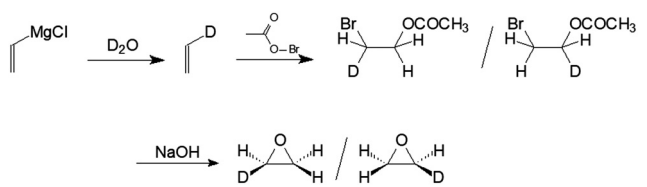

Fig. 2 Synthesis of C_2H_3DO (described in more detail in ref. 14).

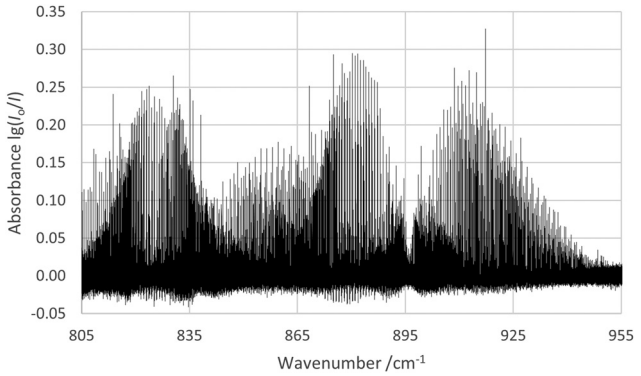

Fig. 3 Overview spectrum of C_2H_3DO as recorded for this study. (T = 295 K, $P \approx$ 1.8 mbar, resolution = 0.0015 cm^{-1}, l = 18 cm). Decadic absorbance $\lg(I_0/I)$ is shown (partial pressure, see text).

however, due to composition. A Globar source was used with an MCT detector and Ge:KBr beam splitters. The spectrometer used was the Bruker IFS 125 HR Zürich Prototype (ZP 2001).[46,47] The final spectrum was obtained by the co-addition of 160 scans and was analyzed in absorbance. Peak positions were determined using the OPUS software supplied by Bruker. The line positions were calibrated ($\Delta\tilde{\nu}_{rms}$ = 0.00006 cm^{-1}) using 41 transitions in the ν_2 fundamental of CO_2[53] present in parts of the spectrum. The calibration shift was small and about constant ($\Delta\tilde{\nu}_{shift} = \tilde{\nu}_{exp} - \tilde{\nu}_{reference}$ = 0.00005 cm^{-1}), which is very small and also consistent with results of a wavenumber calibration performed using a proportional factor. The data in the supplementary publication are presented as calibrated line wavenumbers ($\tilde{\nu}_{obs} = \tilde{\nu}_{exp} - \Delta\tilde{\nu}_{shift}$).

3 Theory

3.1 *Ab initio* calculations

The fully optimized geometry of oxirane has been determined by *ab initio* calculations using Møller–Plesset perturbation theory to second order (MP2) with Gaussian 03 (and subsequent releases)[54] using an augmented, correlation consistent triple-zeta basis set (aug-cc-pVTZ). The vibrational frequencies at the stationary points were all real. Table 1 provides the harmonic ω_i and anharmonic $\tilde{\nu}_i$ fundamentals (in cm^{-1}) for monodeutero-oxirane. The anharmonic analysis is based on second order perturbation theory and obtained from the quartic force field computed with the software from ref. 54. All anharmonic constants are reported in the corresponding table in the ESI.† We also report intensities (calculated in the double harmonic approximation as well as with approximate anharmonic corrections) listed as integrated cross sections $G_i/(pm)^2$ related to the IR intensity $A_i/(km\ mol^{-1})$[55] by eqn (1):

$$G_i/(pm^2) \approx 16.60540 \cdot (A_i/km\ mol^{-1})(\omega_i/cm^{-1}) \quad (1)$$

Here, ω_i is the calculated harmonic vibrational wavenumber (in cm^{-1}). We compare our calculated positions and intensities of the fundamentals for monodeutero-oxirane to those calculated by Puzzarini *et al.*[28] in Table 1.

Table 1 Predicted harmonic wavenumbers ω_i and intensities A_i for monodeutero-oxirane and anharmonic fundamentals $\tilde{\nu}_i$, as well as G_i (in pm^2). Calculations are carried out at the MP2 level with an aug-cc-pVTZ basis set (compared also with the calculated results reported by Puzzarini *et al.* in ref. 28)

Fundamental i	ω_i/cm^{-1} (this work)	A_i/km mol^{-1} (this work)	G_i/pm^2 (this work)	$\tilde{\nu}_i$/cm^{-1} (this work)	$\tilde{\nu}_i$/cm^{-1} CC(VQZ)[28]	A_i/km mol^{-1} (ref. 28)	G_i/pm^2 (ref. 28)
1	3253.318	13.506	0.069	3109.374	3065.3	23.34	0.126
2	3205.911	12.538	0.065	3070.223	3029.6	9.89	0.054
3	3152.067	18.862	0.100	3047.255	3012.2	23.25	0.128
4	2354.197	10.263	0.072	2276.243	2251.3	2.78	0.021
5	1534.503	1.166	0.013	1487.890	1475.4	0.46	0.005
6	1406.279	2.159	0.026	1368.916	1358.4	1.91	0.023
7	1284.669	8.873	0.115	1256.018	1246.7	10.54	0.140
8	1170.365	1.543	0.022	1148.945	1146.4	2.00	0.029
9	1157.065	0.424	0.006	1130.548	1131.8	0.07	0.001
10	1104.401	1.259	0.019	1080.160	1079.1	1.14	0.018
11	1060.128	1.474	0.023	1039.569	1039.6	2.18	0.035
12	916.301	40.817	0.740	894.734	891.7	39.80	0.741
13	853.563	21.433	0.417	836.304	831.4	32.37	0.647
14	840.512	10.010	0.198	817.003	816.7	11.28	0.229
15	714.490	2.545	0.059	704.655	701.2	2.76	0.065

The summary in Table 2 anticipates some of our experimental results, agreeing relatively well with our theoretical results, in which anharmonic corrections are considered in the fundamentals. The agreement is slightly better than for the results of Puzzarini *et al.*[28]

Monodeutero-oxirane is chiral by isotopic substitution, and with one of three distinct isotope effects relevant in high- and ultra-high-resolution spectroscopy,[1,2,5] the parity violating energy difference $\Delta_{pv}E$ between the isotopically chiral enantiomers arises largely from the electroweak interaction between nucleons and electrons.[56,57] Parity-violating potentials V_{pv} have been calculated using the parity violating contribution H_{pv} with the dominant term to the Hamiltonian following[56–58]

$$H_{pv} = \frac{\pi G_F}{hcm_e\sqrt{2}} \sum_{A=1}^{N} Q_A \sum_{i=1}^{n} \left[\vec{p_i}\cdot\vec{s_i}, \delta^3\left(\vec{r_i} - \vec{r_A}\right)\right]_+ \quad (2)$$

$$Q_A \approx Z_A\left(1 - 4\sin^2\Theta_W\right) - N_A \quad (3)$$

where G_F (Fermi constant) is 1.43586×10^{-62} J m^3,[55] m_e is the electron mass, h is Planck's constant, c the speed of light, p_i and s_i are electron momentum and spin operators of electron i at position r_i, and r_A is the position vector of nucleus A. δ^3 denotes the three dimensional Dirac delta distribution, and $[,]_+$ is the anti-commutator. The weak charge Q_A of nucleus A is given by eqn (3) where Z_A is the number of protons, N_A the number of neutrons, and Θ_W the Weinberg angle.[55]

V_{pv} is in principle a multidimensional potential hypersurface depending on the $3N-6$ internal coordinates. The parity violating energy difference $\Delta_{pv}E_{el} = 2|V_{pv}|$ at the equilibrium position ($q = 0$) is about $hc\cdot 2.1 \times 10^{-16}$ cm^{-1}. Within the separable harmonic adiabatic approximation (SHAA) the relative frequency shift for the fundamental ν_{12} can be estimated from the calculated $\Delta\omega/\omega \approx 69 \times 10^{-20}$ whereas a one-dimensional anharmonic approximation (SAAA) gives $\Delta\nu/\nu \approx 64 \times 10^{-20}$.[57,58] Within this approximation and taking only ν_{12} into account one can estimate the ground state energy difference $\Delta_{pv}E_0$. From extensive earlier investigations[56,59,60] it is well established that anharmonic effects on observables influenced by parity violation are most important for stretching vibrations and it is often sufficient to consider anharmonic effects only for the parity conserving potential. Here, the vibrations under consideration are a ring deformation (ν_{12}) and a wagging mode (ν_{13}). In comparison with other molecules for which spectroscopic observables under the influence of parity violation have been investigated,[56,57,61] monodeutero-oxirane shows a rather small relative frequency shift and ground state energy difference arising from parity violation. We report the results here because of their current theoretical interest although they are clearly not detectable in the present spectroscopic experiments.

3.2 Rovibrational Hamiltonian

The rovibrational analysis has been carried out with Watson's *A*-reduced effective Hamiltonian in the I^r representation up to

Table 2 Calculated relative intensities of the nearby fundamentals relative to that of ν_{12}, from this work and the work of Puzzarini *et al.*[28] Comparison between calculated values (harmonic wavenumbers ω_i and anharmonic fundamentals $\tilde{\nu}_i$) from this work and from ref. 28 and experimentally determined band centers for the fundamentals of monodeuterated oxirane in this spectral region, in cm^{-1}

Band		A_i/km mol^{-1} this work (calc.) Harmonic	Anharmonic	A_i/A_{12} (harmonic) (this work)	A_i/A_{12} (anharmonic) (this work)	A_i/km mol^{-1} (ref. 28)	A_i/A_{12} (ref. 28)	ω_i/cm^{-1} this work	$\tilde{\nu}_{calc}$/cm^{-1} (ref. 28)	$\tilde{\nu}_i$/cm^{-1} this work (calc.)	$\tilde{\nu}_{exp}$/cm^{-1} this work
ν_{12}	Ring deform	40.817	37.226	1.000	1.000	39.80	1.000	916.301	891.7	894.734	896.025
ν_{13}	CHD twist	21.433	29.204	0.525	0.785	32.37	0.813	853.563	831.4	836.304	837.363
ν_{14}	Ring deform	10.010	9.917	0.245	0.266	11.28	0.283	840.512	816.7	817.003	—
ν_{15}	CHD rock	2.545	2.629	0.062	0.071	2.76	0.0693	714.490	701.2	704.655	—

sextic centrifugal distortion constants,[62,63] with $i = \sqrt{-1}$.

$$\begin{aligned}\hat{H}^{v,v} = {} & A_v\hat{J}_z^2 + B_v\hat{J}_x^2 + C_v\hat{J}_y^2 - \Delta_J^v\hat{J}^4 \\ & - \Delta_{JK}^v\hat{J}^2\hat{J}_z^2 - \Delta_K^v\hat{J}_z^4 \\ & - \frac{1}{2}\left[\left(\delta_J^v\hat{J}^2 + \delta_K^v\hat{J}_z^2\right), \left(\hat{J}_+^2 + \hat{J}_-^2\right)\right]_+ \\ & + \phi_J^v\hat{J}^6 + \phi_{JK}^v\hat{J}^4\hat{J}_z^2 + \phi_{KJ}^v\hat{J}^2\hat{J}_z^4 + \phi_K^v\hat{J}_z^6 \\ & + \frac{1}{2}\left[\left(\eta_J^v\hat{J}^4 + \eta_{JK}^v\hat{J}^2\hat{J}_z^2 + \eta_K^v\hat{J}_z^4\right), \left(\hat{J}_+^2 + \hat{J}_-^2\right)\right]_+\end{aligned} \quad (4)$$

$$\hat{J}^2 = \hat{J}_x^2 + \hat{J}_y^2 + \hat{J}_x^2 \quad (5)$$

$$\hat{J}_\pm = \hat{J}_x \pm i\hat{J}_y. \quad (6)$$

We have also examined a possible Coriolis interaction between ν_{12} and ν_{13} states and have expressed this interaction as

$$\hat{H}_{\text{rot}}^{v'v} = i\xi_\alpha^{v'v}\hat{J}_\alpha + e_{\beta\gamma}^{v'v}\left[\hat{J}_\beta, \hat{J}_\gamma\right]_+ \quad (7)$$

with $(\alpha, \beta, \gamma) = (x, y, z)$ all different and using here the symbol e instead of the more common η, (see ref. 47, 63 and 64).

The rotational constants A, B, C, the quartic centrifugal distortion constants Δ_J^v, Δ_{JK}^v, Δ_K^v, δ_J^v and δ_K^v and the sextic centrifugal distortion constants ϕ_J^v, ϕ_{JK}^v, ϕ_{KJ}^v, ϕ_K^v, η_J^v, η_{JK}^v and η_K^v depend upon the vibrational level v. Here, $[,]_+$ is the anticommutator and $[,]_-$ is the commutator. We prefer the notation with the Greek η here, because the also quite commonly used lower case Greek phi ϕ can be confused with the upper case phi (Φ). The spectroscopic data have been analyzed with a least squares fit using the WANG program, described in detail in ref. 64. Extensive background information on the applications of WANG is also available in the literature.[47,63,65] For comparison, we have also used the program SPFIT developed later by Pickett,[66] and for some of the graphics PGOPHER.[67] When used with the same effective Hamiltonians, the two programs give almost identical results, with occasional small numerical differences of no physical significance.

4 Vibrational ground state of c-C_2H_3DO revisited

In the course of the present work on the spectra of excited vibrational states of c-C_2H_3DO, we have extended substantially the assignment of rotational transitions in the FT-THz spectra measured with our spectrometer at the Swiss Light Source (SLS) in our previous work.[14]

We were able to assign about 1000 further transitions in these spectra in the range from 0.75 to 1.84 THz in addition to the 398 previous assignments in this range.[14] We have noted that inadvertently in the previous publication some uncorrected tables with misprints and results from preliminary preconverged fits of the data were represented. While this does not affect the original spectra and corresponding data and conclusions, as the changes are not large, in general, we reproduce here in the ESI† a set of the corresponding corrected tables (labeled as C1 and C2 (2019) for the tables in the main text part and Table CS1, CS2, CS3 (2019) for the supplementary tables (ESI†) also Fig. S1, S2, S3, S4 (2019)), although the changes in these are hardly visible. In the previous supplementary tables (ESI†) we also had truncated the wavenumber data for the observed lines presented in cm^{-1} units at the 5th digit after the decimal point (*i.e.* to 0.00001 cm^{-1}). While this precision would be adequate for the FT-THz values, it may not be adequate for further use of the GHz data, which are actually more precise. Thus, in the corrected tables we report all the previously observed line data in MHz to four digits after the decimal point (*i.e.* 0.1 kHz), which is well below the experimental uncertainty of the data and sufficiently numerically precise for most purposes. These experimental data are now given in Table CS2 (ESI†) (the data truncated in cm^{-1} as before would be the same as in S2(2019)). Recently the work of Müller *et al.*[17] has also added more than one thousand newly measured lines in the submm range (0.491 to 1.06 THz) to the data set for the vibrational ground state of c-C_2H_3DO.

Table 3 provides a survey of all currently available data for this state, as well as various previous and present analyses and fits of these data, with relative weights assigned according to the reciprocal of the estimated uncertainty of the corresponding experimental data. Müller *et al.*[17] have already provided a combined fit of their new and our previous data (communicated by us to them at higher precision than given by the truncated values in the previously published tables). We have reproduced their fit using their selected combined dataset, which included our 2019 results. We give the result of this fit in column 3 of Table 4. The result agrees perfectly except for deviations in one unit of the last digit for a few parameters, far below the uncertainty, below one tenth of the 1σ uncertainty, resulting from small numerical effects and not physically significant. In their analysis, Müller *et al.*[17] recalibrated our previous FT-THz results with an average recalibration factor of 1.0000037 leading to a very slight shift of our original data. We have in our own final global analysis not used such a recalibration but rather used our original FT-THz values as they were calibrated in a standard way using water lines appearing *in situ* in our spectra.[68] This calibration shift in any case is very small, ranging from 0.00007 at 25 cm^{-1} to 0.00010 at 50 cm^{-1}. With the most recent data from the HITRAN data set[69] one would obtain different shifts, but it is not clear whether this would provide an improvement. The uncertainty in the calibration data is estimated to be about 0.0001 cm^{-1}, although it may actually be larger. Müller *et al.*[17] have also argued that an effective Hamiltonian using Watson's *S*-reduction and the III^l representation gives a better fit than the use of the *A*-reduction with the I^r-representation as used by us before. While we were able to reproduce their III^l fit as well, in essence, the minimal improvement occurs only in the GHz and MW data and disappears when all data are considered. Indeed, c-C_2H_3DO is a highly asymmetric rotor with an asymmetry parameter $\kappa = 0.204$[70] which is closer to zero than it is to +1 (oblate limit) or to −1 (prolate limit). The choice of reduction and representation is not *a priori* obvious and is rather arbitrary. In any case, the parameters of the effective Hamiltonians do not have much physical significance in terms of

Table 3 Summary of data analyzed in the current evaluation

Range/GHz	N_{trans}[a]	N_{freq}[b]	$K_{a,max}$	$K_{c,max}$	J_{max}	Rel. weight	Ref.
10–60 (MW)	20	20	5	4	8	20	[Hirose][f]
60–120 (GHz)	112	112	14	10	23	200	[Albert *et al.*][g]
750–2090 (FT-THz)	398	398	40	58	58	0.42	[Albert *et al.*][g]
491–1060 (submm)	1506	1091	58	43	55	33.3–200	[Müller *et al.*][h]
41–297 (IR GSCD)	325[c]	310	30	41	42	0.21	This work
750–1840 (FT-THz)	1409[d]	848	38	57	57	0.42	This work
10–1840 (global)	3370[e]	2379	58	43	57		This work

[a] Number of transitions used in the fit. [b] Number of distinct frequencies used in the fit. [c] Combination differences from rovibrational analyses of IR spectra in the range of 800–950 cm^{-1}. [d] The FT-THz data of 2019 were reanalyzed and combined with the new data set of 2023 for the selected data set in the final fit. [e] This is the data set which was selected in our final fit combining data from all sources, but not retaining all of them in the final fit, see text. [f] Hirose, 1974.[43] [g] Albert *et al.*, 2019.[14] [h] Müller *et al.*, 2023.[17]

a simple model interpretation. They are "effective parameters" in the proper sense of the word (see also the discussion in ref. 63).

Indeed, we are able to provide an adequate fit of all current data, including also our new data, using an *A*-reduced Hamiltonian in the I^r representation using a small parameter set including only up to sextic constants as we used it before.[14] The result of our new global analysis, which includes more than 1000 newly assigned rotational transitions and almost 400 combination differences obtained from the analyses of the vibrational spectra discussed in detail below, are shown in columns 4 and 5 of Table 4 obtained with a large parameter set (LP) and a small parameter set (SP). We thus consider the result in the last column (5) in Table 4 to be a best compromise choice. These parameters for the vibrational ground state provide a good starting point in the analysis of the spectra of excited vibrational states. This effective Hamiltonian incorporates effects from the omitted higher order parameters in the low order parameters, which therefore differ slightly between

Table 4 Spectroscopic constants for the ground state of monodeutero-oxirane in the MW, GHz and THz ranges (values in parenthesis provide statistical 1σ uncertainties in units of the last specified digits)

	MW, GHz, THz combined[a] C2019	MW, GHz, sub-mm, THz combined[d] MNRAS2023	All rotational transitions[e] global fit (SPFIT) LP This work	All rotational transitions[e] global fit (WANG) SP This work
A/MHz	24 252.6477(44)[b]	24 252.647815(44)	24 252.647835(43)	24 252.64570(15)
B/MHz	19 905.5213(44)	19 905.523291(40)	19 905.523330(39)	19 905.52270(20)
C/MHz	13 327.5813(44)	13 327.583649(53)	13 327.583701(52)	13 327.58370(16)
Δ_J/kHz	17.0779(35)	17.04198(11)	17.04211(11)	17.04117(26)
Δ_K/kHz	25.458(19)	25.46266(18)	25.46261(18)	25.45675(24)
Δ_{JK}/kHz	17.275(19)	17.25673(12)	17.25667(12)	17.25473(26)
δ_J/kHz	4.7418(17)	4.742161(17)	4.742156(17)	4.741796(42)
δ_K/kHz	13.2423(85)	13.231691(56)	13.231664(55)	13.23277(11)
ϕ_J/mHz	13.9(12)	12.36(10)	12.50(10)	11.697(95)
ϕ_{JK}/mHz	219(15)	141.97(15)	141.92(15)	138.67(17)
ϕ_{KJ}/mHz	−1006(37)	−835.25(36)	−835.38(35)	−829.84(22)
ϕ_K/mHz	910(29)	808.08(30)	808.11(30)	797.41(14)
η_J/mHz	2.2[c]	4.797(13)	4.794(13)	4.602(15)
η_{JK}/mHz	81.1[c]	62.667(69)	62.640(68)	62.056(62)
η_K/mHz	61.7[c]	30.21(10)	30.17(10)	33.301(74)
L_K/Hz	—	−9.13(24)	−9.15(24)	—
L_{KKJ}/Hz	—	6.51(27)	6.52(27)	—
L_{JK}/Hz	—	1.55(19)	1.61(19)	—
L_{JJK}/Hz	—	−2.099(64)	−2.087(63)	—
l_J/Hz	—	−0.169(30)	−0.212(30)	—
l_K/Hz	—	−4.571(60)	−4.587(59)	—
l_{KJ}/Hz	—	2.243(41)	2.262(40)	—
l_{JK}/Hz	—	−1.191(24)	−1.183(24)	—
$l_J/10^{-3}$ Hz	—	−34.7(36)	−34.5(35)	—
$P_K/10^{-3}$ Hz	—	1.30(10)	1.27(10)	—
$P_{KKJ}/10^{-3}$ Hz	—	−1.94(17)	−1.87(17)	—
$P_{KJ}/10^{-3}$ Hz	—	0.851(99)	0.798(98)	—
d_{rms}/MHz	2.290	2.405	2.6797	2.501
n_{data}	530	2418	3370	3370

[a] Based on spectra reported in Albert *et al.*[14] in 2019 (as corrected here as C2019). [b] Values in parenthesis indicate uncertainties as 1σ in units of the last digits given. Rotational constants in C2019 were held fixed to the respective values of the ground state obtained by fitting only transitions in the GHz region of this study, to which the uncertainties given correspond. [c] Fixed at the *ab initio* estimate from Puzzarini *et al.*[28] [d] Reproduced from data reported in Müller *et al.*[17] as MNRAS2023. [e] All FT-THz transition wavenumbers were converted to frequencies in MHz in the data set. LP: large parameter set; SP: small parameter set, see also discussion in the text.

the LP and the SP Hamiltonians. However, such an effective Hamiltonian with a small number of parameters, while not providing the highest precision for all data, provides more stability in predictions, being less sensitive to artifacts arising when extrapolating with many high order parameters of non-negligible uncertainties. We note that the apparent contradiction of a slightly larger root mean square deviation d_{rms} for LP and SP on the same data set (see columns 4 and 5) arises from the actual weighting of the data in the fit, whereas d_{rms} is calculated here as an unweighted result. We have also found that the program SPFIT[66] converges apparently on a slightly less favourable minimum in the fit than WANG[64] (see also supplementary tables, ESI†). The slight differences have no physical significance (as described elsewhere[63,71]). We note that slight differences in the parameters arise even with a use of the same program, when changing the input for transitions from cm^{-1} to Hz units by multiplication with the speed of light. While physically identical by definition, the results of the fits are not numerically identical, with small differences, which have no physical significance.

In our final new global fits we did not retain all lines of the previous data set, but excluded those which have relatively large uncertainties when they arise from blended or very weak lines. For instance, the new data set of 1409 original FT-THz transitions includes many but not all of the 2019 FT-THz data (398). The actually selected data set of 3370 assigned transitions is apparent from the table in the ESI.† The last line in Table 3 thus does not simply arise as a sum of the values in the lines above it. In order to characterize further the quality of the parameter adjustment in representing the data globally, we note the absolute values of the maximum deviations of observed and calculated lines (0.026 MHz for the GHz data,[14] 0.646 MHz for the GHz data,[17] 8.96 MHz for the FT-THz, and 23.9 MHz for the GSCD which have the largest uncertainty).

Of the 3370 transitions, only 55 FT-THz deviate by more than $|\Delta\nu|$ = 5 MHz and 123 for the ground state combination differences (GSCD, none for GHz and MW). Deviations larger than 10 MHz occur only for the GSCD data. As an example of a comparison of experimental primary data and simulations we show in Fig. 4 a small region of the experimental FT-THz spectrum compared with several simulations. The agreement is very good and similar for all three simulations (extra lines arise from other isotopomers, hot bands, and impurities as discussed before[14]). In the ESI,† we show further examples of experimental and simulated spectra with similar conclusions. For completeness, we show here in Table 5 the predicted frequencies for the lines identified by Müller *et al.*[17] in the astrophysical spectra. The column "Identified" provides the predicted frequencies of the Hamiltonian of Müller *et al.* identified in the astrophysical observations. The other columns give the predictions from the 2019 data (C2019) and current results using the large parameter set (LP2025) and the small parameter set (SP2025). The differences are very small, usually below 0.1 MHz and always below 1 MHz, thus not really significant for this application.

5 Assignment for excited vibrational states and results

The assignment of over 1100 rovibrational transitions belonging to particular subbands of ν_{12} and ν_{13} consisting of *P* and *R* branches has been carried out efficiently with the interactive Giessen Loomis-Wood assignment program[72] and with the Zürich program LOOM4WANG.[63] The Loomis-Wood method, previously extensively used for the assignment of linear molecules,[73] has been used successfully for several asymmetric top molecules $CH^{35}Cl_2F$,[74] CDBrClF[46] and $CHClF_2$[75] because these molecules display symmetric top behavior (no observable

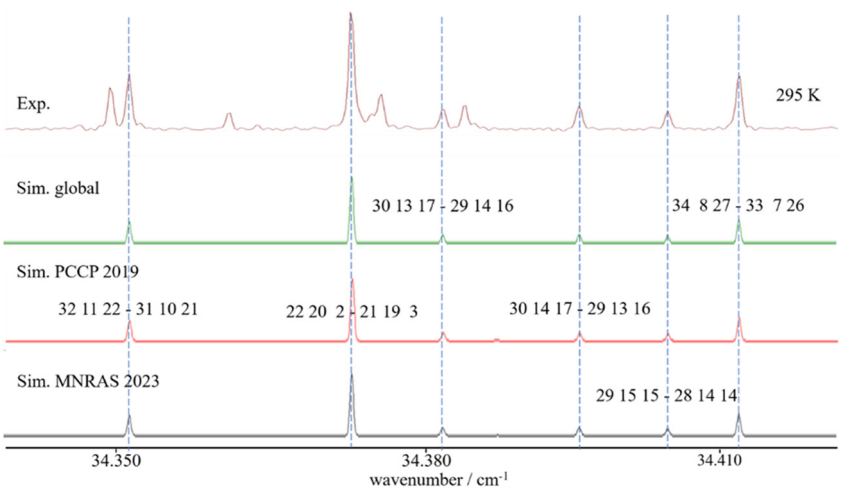

Fig. 4 A comparison of the THz spectrum of monodeutero-oxirane (from top to bottom): (1) observed spectrum; (2) simulated spectrum based on the global analysis of this study (Table 4, column 4); (3) simulated spectrum reproduced using data in Albert *et al.*[14] (Table 5, column 1); (4) simulated spectrum reproduced using data in Müller *et al.*[17] (Table 5, column 2). Quantum numbers of transitions are arranged in the form of $J'K'_aK'_c - J''K''_aK''_c$. Absorbance is shown in relative units for illustration.

Table 5 Predicted frequencies for identified transition frequencies of D_1-oxirane in MHz

						Identified	Predicted frequencies		
J'	K'_a	K'_c	J''	K''_a	K''_c	MNRAS2023[a]	C2019[b]	LP2025	SP2025
5	5	1	4	4	0	235 180.99	235 180.966	235 180.993	235 180.977
22	8	14	22	7	15	235 190.43	235 190.334	235 190.428	235 190.421
22	9	14	22	8	15	235 200.38	235 200.288	235 200.382	235 200.375
5	5	0	4	4	1	235 965.82	235 965.795	235 965.823	235 965.807
9	5	5	8	4	4	331 568.82	331 568.679	331 568.820	331 568.805
10	5	5	9	6	4	332 130.07	332 129.880	332 130.068	332 130.080
7	7	1	6	6	0	332 520.25	332 520.181	332 520.251	332 520.232
7	7	0	6	6	1	332 594.25	332 594.177	332 594.248	332 594.229
11	2	9	10	3	8	335 611.61	335 611.599	335 611.835	335 611.835
11	3	9	10	2	8	335 620.97	335 620.737	335 620.973	335 620.972
7	4	3	6	3	4	337 191.43	337 191.354	337 191.432	337 191.420
10	4	6	9	5	5	338 717.98	338 717.793	338 717.979	338 717.979
12	1	11	11	2	10	345 236.98	345 236.689	345 236.984	345 236.985
12	2	11	11	1	10	345 237.01	345 236.717	345 237.013	345 237.014
8	6	3	7	5	2	346 866.07	346 865.973	346 866.075	346 866.056
10	5	6	9	4	5	350 271.77	350 271.581	350 271.767	350 271.757
11	3	8	10	4	7	352 688.86	352 688.627	352 688.864	352 688.863
11	4	8	10	3	7	352 939.91	352 939.678	352 939.915	352 939.913
10	6	5	10	7	4	353 520.70	353 520.462	353 520.698	353 520.718
13	1	13	12	0	12	354 922.73	354 922.366	354 922.732	354 922.734
13	0	13	12	1	12	354 922.73	354 922.366	354 922.732	354 922.734
8	6	2	7	5	3	358 772.79	358 772.683	358 772.790	358 772.774
12	2	10	11	3	9	362 232.22	362 231.924	362 232.220	362 232.220
12	3	10	11	2	9	362 233.93	362 233.635	362 233.930	362 233.931

[a] Müller *et al.*, 2023[17] [b] Albert *et al.* 2019.[14]

asymmetry splitting) at higher J levels. An extensive overview of the development and current use of Loomis-Wood programs is available in ref. 63.

The assignments were confirmed using combination differences (GSCD) and the ground state energy level values available from Section 4. The overwhelming majority of the ν_{12} and ν_{13} transitions observed here were from unresolved doublets with degenerate K_a values ($K_a = J - K_c$ and $K_a = J - K_c + 1$) or K_c values ($K_c = J - K_a$ and $K_c = J - K_a + 1$). The transitions belonging to the ν_{12} band were fit initially, including up to the quartic centrifugal distortion constants, initially using $J < 20$ transitions (ν_{12}: 325 transitions) to determine molecular parameters for the molecule as outlined above. The observed minus calculated values $\Delta\tilde{\nu} = \tilde{\nu}_{obs} - \tilde{\nu}_{calc}$ for the line positions are shown in Fig. 5. The fit was then extended to fit the entire 825 transitions assigned for ν_{12}. The deviations between observed and calculated transitions for higher J and K_a quantum numbers increased with increasing J and K_a values.

This behavior indicated a possible Coriolis resonance between the ν_{12} and nearby states, particularly the ν_{13} state at 837 cm^{-1}. The transitions associated with the ν_{13} band were then assigned and included in the fit. Initially, the 230 ν_{13} transitions with $J < 20$ were analyzed separately, before including higher J value transitions in the fit. The presence of interactions between ν_{13} and other states was already indicated in the diagrams of the observed-calculated line positions for lines with $J < 20$ (Fig. 6).

The analysis was then carried out for both bands simultaneously using all assigned transitions: (ν_{12}: 825 transitions and ν_{13}: 323 transitions, total = 1148 transitions), providing a better

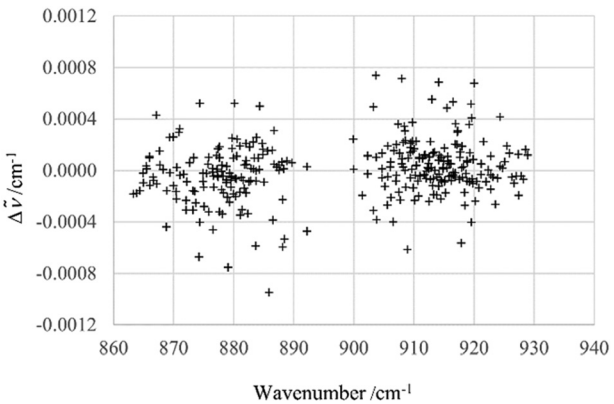

Fig. 5 $\Delta\tilde{\nu} = \tilde{\nu}_{obs} - \tilde{\nu}_{calc}$ for ν_{12} transitions ($J < 20$). Calculated values were obtained using the effective Hamiltonian described in the text.

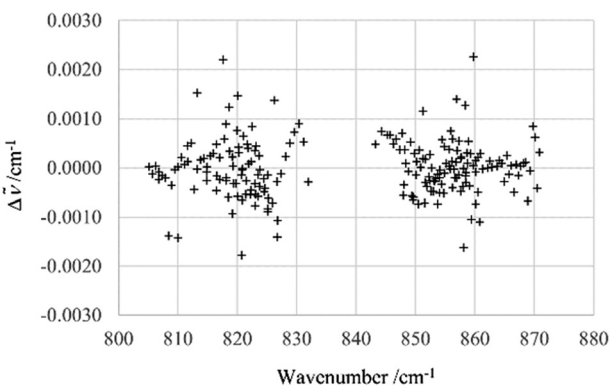

Fig. 6 $\Delta\tilde{\nu} = \tilde{\nu}_{obs} - \tilde{\nu}_{calc}$ for ν_{13} transitions ($J < 20$). Calculated values were obtained using the effective Hamiltonian described in more detail in the text.

Table 6 Molecular parameters (in cm^{-1}) of the ν_{12} and ν_{13} states of monodeutero-oxirane

	Fit separately, no interaction included		Coriolis interaction included		
Parameter	ν_{12} (separate)	ν_{13} (separate)	ν_{12}	ν_{13}	Ground state[a]
ν_0/cm^{-1}	896.025095(45)	837.36315(65)	896.02513(17)	837.36303(36)	—
A/cm^{-1}	0.80716728(40)	0.808361(12)	0.80694(14)	0.80859(14)	0.808981182
B/cm^{-1}–	0.66274527(84)	0.663813(20)	0.6627467(33)	0.663822(11)	0.663976767
C/cm^{-1}	0.449280716(23)	0.4530818(76)	0.4492788(14)	0.4530821(42)	0.44456034
$\Delta_J/10^{-6}$ cm^{-1}	0.8004(18)	3.292(73)	0.8021(67)	3.398(39)	0.568432245
$\Delta_K/10^{-6}$ cm^{-1}	1.08060(42)	4.17(24)	1.082(16)	4.44(13)	0.849145778
$\Delta_{JK}/10^{-6}$ cm^{-1}	0.0286(60)	−5.99(29)	0.034(23)	−6.36(16)	0.576555584
$\delta_J/10^{-6}$ cm^{-1}	0.03073(88)	−1.159(36)	0.0326(35)	−1.110(19)	0.158169289
$\delta_K/10^{-6}$ cm^{-1}	0.7022(15)	3.977(96)	0.6953(73)	4.105(50)	0.441397695
$\phi_J/10^{-12}$ cm^{-1}	18(2)	990(190)	18(8)	1534(69)	0.390169922
$\phi_{JK}/10^{-12}$ cm^{-1}	−67(7)	−3570(880)	−74(28)	−5070(450)	4.62553331
$\phi_{KJ}/10^{-12}$ cm^{-1}	118(5)	4800(120)	139(21)	3910(600)	−27.6804829
$\phi_K/10^{-12}$ cm^{-1}	−70(4)	−2650(800)	−83(16)	−790(260)	26.5987345
$\eta_J/10^{-12}$ cm^{-1}	−12(1)	−650(93)	−11(4)	−381(33)	0.153506197
$\eta_{JK}/10^{-12}$ cm^{-1}	50(1)	2600(270)	50(5)	2880(140)	2.06996535
$\eta_K/10^{-12}$ cm^{-1}	−94(5)	−3700(740)	−103(21)	−1540(200)	1.11080179
ξ_z/cm^{-1}	—	—	0.116(34)	—	
n_{data}	825	323	1148	—	
d_{rms}/cm^{-1}	0.0003101	0.002132	0.001176	—	

[a] Fixed (see Table 4).

estimate of molecular parameters for ν_{12} and ν_{13} and providing an estimate of the Coriolis interaction between the two upper states. The difference $\Delta\tilde{\nu} = \tilde{\nu}_{observed} - \tilde{\nu}_{calculated}$ between the observed spectrum and a spectrum calculated using the molecular parameters in Table 6 is shown in Fig. 7.

The reduced term values were calculated and examined for further insight into the resonance between ν_{13} and an as yet unassigned resonance partner, possibly ν_{14} (predicted to be near 817 cm^{-1}). The reduced term values were calculated by first finding the energy of the upper vibrational level (the transition plus the ground state energy level for J'' K_a'' and K_c'') and then subtracting the energy of the ground state energy level with J'', K_a'' and K_c''. It is apparent that the higher $K_a = n$ states (n = 1, 2, 3) are perturbed, even at low J. This explains the difficulties encountered even while fitting only the lower J value transitions of this band, and the large residuals observed for the ν_{13} transitions in Fig. 6 and 7. In addition, the calculated relative intensity values (anharmonic *vs.* harmonic) differ significantly for ν_{12} and ν_{13} (Table 2): this is as would be expected in light of the interactions present. Illustrated in Fig. 8 and 9 are direct comparisons between the observed spectrum (black) and the spectrum as calculated (red) using the effective Hamiltonian

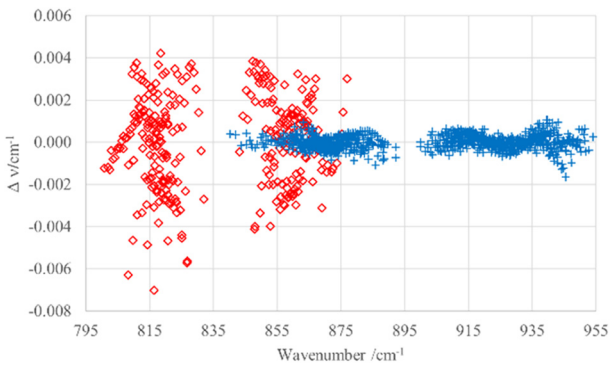

Fig. 7 $\Delta\tilde{\nu} = \tilde{\nu}_{obs} - \tilde{\nu}_{calc}$ for ν_{12} and ν_{13} transitions, including high-J transitions, together with the introduction of a Coriolis interaction. ν_{12}: blue cross; ν_{13}: red box. (The least squares fit was performed using the effective Hamiltonian described in more detail in the text).

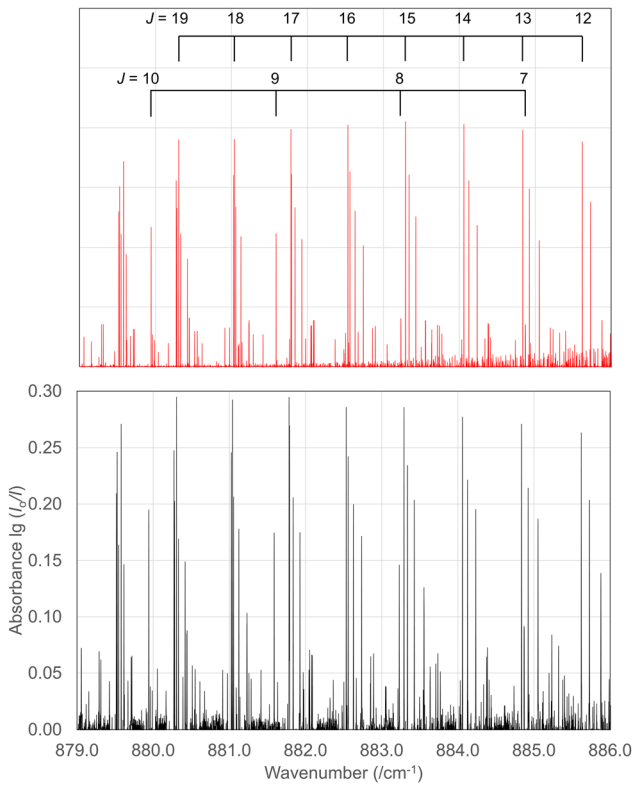

Fig. 8 Comparison of measured (black) and calculated (red) P branch transitions in the ν_{12} fundamental of c-C_2H_3DO. The assignments are shown in the figure. Transitions associated with J = 12–19 in the K_a = 0 series (upper comb) and with J = 7–10 in the K_c = 0 series (lower comb) are shown. Decadic absorbance is shown $lg(I_0/I)$.

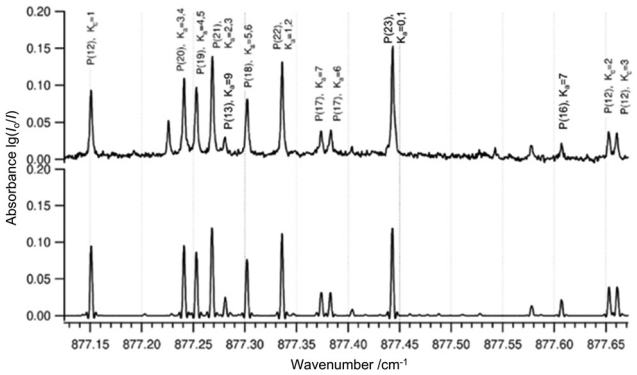

Fig. 9 Comparison of an extended section of the measured P branch transitions (top trace, T = 295 K, l = 18 cm, $P \approx$ 1.8 mbar, nominal instrumental resolution 0.0015 cm^{-1}) in the ν_{12} fundamental of c-C_2H_3DO with a spectrum calculated using the molecular parameters in Table 6 (columns 4–6) and a Gaussian line width with $\Delta\tilde{\nu}_{calc}$(FWHM) = 0.0015 cm^{-1}. The effective linewidth $\Delta\tilde{\nu}_{FWHM} \approx$ 0.0025 cm^{-1}, typically, for isolated lines in the spectrum. The assignments of the transitions are indicated in the figure. Decadic absorbance lg(I_0/I) is shown.

and the parameters in Table 6 (columns 4–6) (bottom trace). Fig. 8 shows a section of the ν_{12} P-branch region, with the assignments for the K_a and K_c series indicated on the combs above the spectrum. A detailed view of part of the ν_{12} P-branch region, including assignments, is shown in Fig. 9, see also the overview in Fig. 10.

Initially, the spectroscopic constants of Watson's A-reduced effective Hamiltonian in the I^r representation for the ν_{12} state of c-C_2H_3DO were determined. Next, the transitions identified as belonging to the weaker ν_{13} band were assigned and fit separately (see Fig. 11). Then, these were added in a stepwise fashion into the analysis of the ν_{12} fundamental. The sextic parameters ϕ_J, ϕ_{KJ}, ϕ_{JK} and ϕ_K of Watson's A reduced effective Hamiltonian were determined, and the Coriolis interaction between the ν_{12} and the ν_{13} state was estimated.

We first included only ξ_z in the fit, obtaining a value of 0.116 cm^{-1} for this parameter, compared to an *ab initio* estimate of ξ_z = 0.3. Fixing the parameter at this *ab initio* value gives an adequate but somewhat less good fit. We also carried out fits adjusting both ξ_z and e_{xy}, which improved the fit further, but still with limited physical significance. Given the relatively large uncertainties in the sextic parameters (ϕ, η) we also tried to fix these at their ground state values and adjusted only up to the quartic parameters. This, however, resulted in significantly less good representations of the experimental data. We thus consider the two options for sets of effective Hamiltonian parameters to be a reasonable compromise to best represent the experimental data. This improved the root mean square deviation to d_{rms} = 0.001164 cm^{-1}. Nevertheless, it should be clear that the sextic parameters obtained in this way have large uncertainties and very limited physical significance, being "effective" parameters only (see also below). The transitions used in the fit are listed in the ESI† for this paper. Table 6 presents the parameters obtained for the excited vibrational states. The complete tables of the assigned lines can

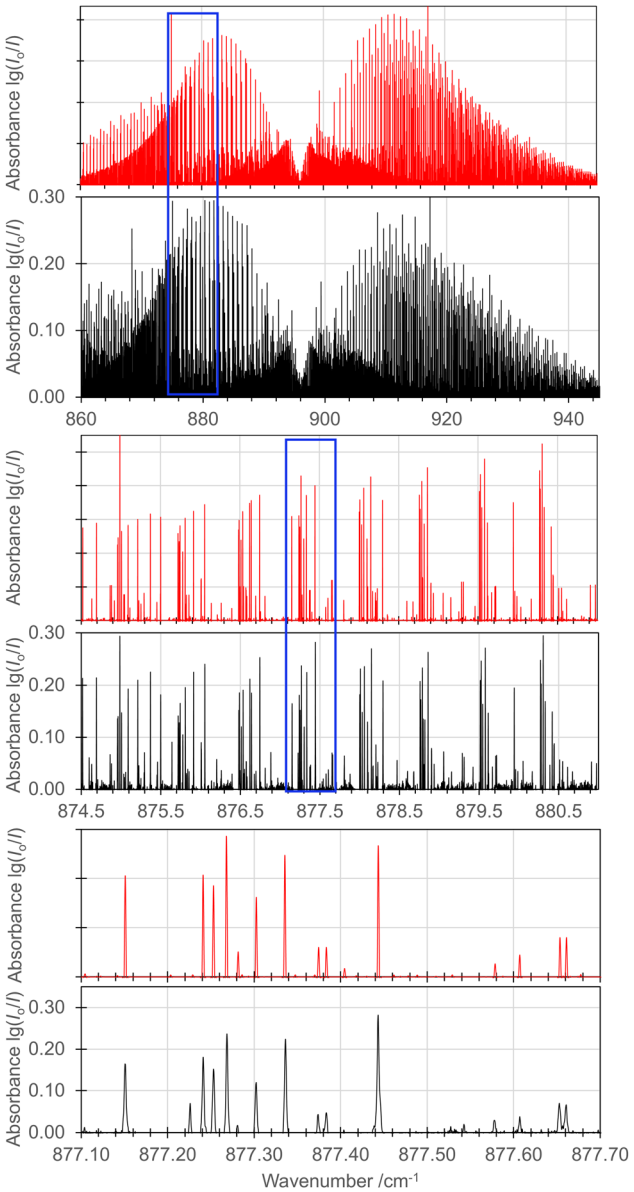

Fig. 10 Overview spectrum of the ν_{12} fundamental illustrating the calculated (red, top traces) and experimental (black, bottom traces) spectrum. The experimental spectrum (black, bottom) was measured with l = 18 cm, $P \approx$ 1.8 mbar, and nominal instrumental resolution 0.0015 cm^{-1}. The calculated spectrum (red, top) was calculated using the molecular parameters in Table 6 (columns 4–6) and a Gaussian line width with $\Delta\tilde{\nu}_{calc}$(FWHM) = 0.0015 cm^{-1}. Decadic absorbance lg(I_0/I) is shown.

be found in the ESI.† It is important to note that these two fundamentals are not the only ones in this part of the infrared spectrum. As is seen in Table 1, the ν_{14} fundamental with a predicted band center around 817 cm^{-1} might also be interacting with ν_{13} and ν_{12}: this band is significantly weaker and must be characterized to complete the analysis of the polyad spectrum in this region. Furthermore, the lowest fundamental, ν_{15}, is also close, with possible further interactions. The parameters presented in Table 6 should thus be considered "effective" parameters including the influence of such interactions. The

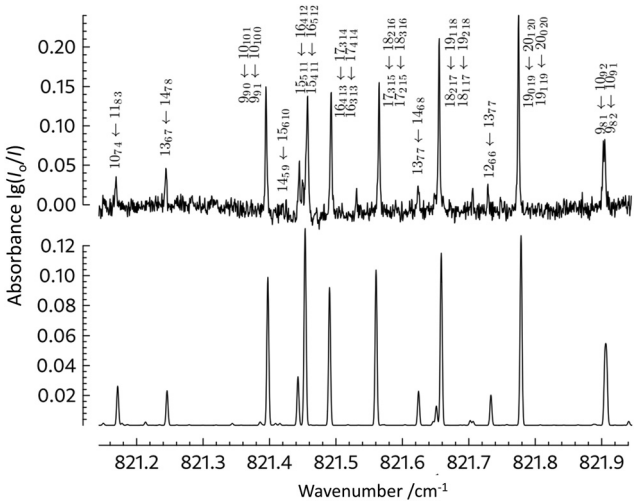

Fig. 11 Comparison of an extended section of the measured *P*-branch transitions (top trace, T = 295 K, l = 18 cm, $P \approx$ 1.8 mbar, nominal instrumental resolution 0.0015 cm^{-1}) in the ν_{13} fundamental of *c*-C_2H_3DO with a spectrum calculated using the molecular parameters in Table 6 (columns 4–6) and a Gaussian line width with $\Delta\tilde{\nu}_{calc}$(FWHM) = 0.0015 cm^{-1}. The effective linewidth (full width at half maximum) $\Delta\tilde{\nu}_{FWHM} \approx$ 0.0025 cm^{-1}, typically, for isolated lines in the spectrum. The assignments of the transitions are indicated in the figure. Decadic absorbance lg(I_0/I) is shown.

analysis of overlapping bands, as well as that of additional measurements of monodeuterated oxirane up to 3600 cm^{-1}, is in progress and will be the subject of future publications.

The spectrum of *c*-C_2H_3DO in this region was simulated based on the parameters given in Table 6 (columns 4–6). Fig. 10 illustrates successive enlargements of the ν_{12} band in the *P* branch region. The extra transitions which cannot be reproduced by the simulation are associated with the undeuterated or doubly deuterated isotopomers *c*-C_2H_4O and *c*-$C_2H_2D_2O$, or in some cases with dichloromethane, which were all present as impurities in the sample, without affecting the high-resolution analyses of the spectra.

6 Discussion and conclusions

High resolution spectroscopy provides one of the most powerful techniques to study the structure and dynamics of polyatomic molecules.[76,77] It also allows us to identify structures in remote locations, from the Earth's atmosphere[78] to interstellar space.[79] Notably, for chiral structures there is so far little information available about their prevalence in the interstellar medium, and D_1-oxirane is so far the only isotopically chiral molecule identified by astrophysical spectroscopy and, with the related methyl oxirane,[80] one of so far overall two chiral structures identified in the interstellar medium. On the other hand, D_1-oxirane can also be related to its achiral isomers with the relevant isotopomers of acetaldehyde (CH_3CHO) vinyl alcohol (CH_2CHOH) or methylhydroxycarbene (CH_3COH), which are all interesting candidates for detection by astrophysical spectroscopy. In addition, detecting chiral compounds by planetary or interstellar spectroscopy opens a route towards detecting enantiomeric excess by means of high resolution vibrational circular dichroism spectra as proposed in ref. 22 as a possible signature of life (see also ref. 81–83). While this goes beyond current astrophysical detection, it provides further motivation for the future high-resolution study of such structures.[22]

Building on our previous work on the GHz and THz far infrared rotational spectra of monodeutero-oxirane,[14] we have obtained here a first analysis of high resolution rotation–vibration spectra of this molecule. This paves also the way for future astrophysical observations in the infrared region of the spectra which may become possible.[18–21] The present analysis of the ν_{12} and ν_{13} fundamentals provides sufficiently accurate effective Hamiltonian parameters for the representation of the spectra including interpolation of data in the observed ranges of quantum numbers. At the same time, we have extended the boundaries of our accurate knowledge of the spectrum of the vibrational ground state, which can provide a benchmark for such a small to medium size molecule.

Future work in our currently ongoing investigations aims at extending the analysis to the lower frequency fundamentals ν_{14} and ν_{15}, as well as further fundamentals extending into the mid to near infrared, and to further chiral isotopomers.[15] Finally, fundamental studies of parity violation in chiral molecules will profit from the high resolution results of the present work.[1–5] Also, monodeutero-oxirane is sufficiently small to serve as a benchmark molecule for theories relating spectra of chiral molecules to their quantum structure and dynamics by full-dimensional rotation–vibration calculations including even parity violation.[56–60,84–88]

Data availability

All relevant data are included in the ESI.†

Conflicts of interest

There are no conflicts to declare.

Acknowledgements

Financial support by the Schweizerischer Nationalfonds (including support initially under the Marie Heim-Vögtlin Program and grant no 200021-207787), ETH Zürich, an ERC Advanced Grant, COST MOLIM, COST COSY and the AGS (Alliance for Global Sustainability) is gratefully acknowledged, as well as help from and discussions with Carine Manca Tanner, Eduard Miloglyadov, Andreas Schneider, Georg Seyfang, Guido Grassi, Reto Ulrich, Daniel Zindel and Fabian Hobi, and Leon Becht, and in particular also continued support from Frédéric Merkt.

References

1 M. Quack, *Angew. Chem.*, 1989, **101**, 588 (*Angew. Chem., Int. Ed. Engl.*, 1989, **28**, 571).
2 R. Berger, G. Laubender, M. Quack, A. Sieben, J. Stohner and M. Willeke, *Angew. Chem.*, 2005, **117**, 3689 (*Angew.*

Chem., Int. Ed., 2005, **44**, 3623); see also A. Sieben, R. Berger, M. Quack and M. Willeke, *Proc. 18th Coll. High Resol. Mol. Spectroscopy*, Dijon, paper F4, 2003, p. 161.
3 M. Hippler, E. Miloglyadov, M. Quack and G. Seyfang, Mass and Isotope Selective Infrared Spectroscopy, in *Handbook of High-Resolution Spectroscopy*, ed. M. Quack and F. Merkt, Wiley, Chichester, 2011, vol. 2, pp. 1069–1118.
4 M. Quack, G. Seyfang and G. Wichmann, *Chem. Sci.*, 2022, **13**, 10598.
5 M. Quack, Fundamental Symmetries and Symmetry Violations from High Resolution Spectroscopy, in *Handbook of High-Resolution Spectroscopy*, ed. M. Quack and F. Merkt, Wiley, Chichester, 2011, vol. 1, pp. 659–722.
6 M. Quack, *Chem. Phys. Lett.*, 1986, **132**, 147.
7 J. E. Dickens, W. M. Irvine, M. Ohishi, M. Ikeda, S. Ishikawa, A. Nummelin and A. Hjalmarson, *Astrophys. J.*, 1997, **489**, 753.
8 A. Nummelin, J. E. Dickens, P. Bergman, A. Hjalmarson, W. M. Irvine, M. Ikeda and M. Ohishi, *Astron. Astrophys.*, 1998, **337**, 275.
9 M. Ikeda, M. Ohishi, A. Nummelin, J. E. Dickens, P. Bergman, A. Hjalmarson, W. M. Irvine and S. Ishikawa, *Astrophys. J.*, 2001, **560**, 792.
10 M. A. Requena-Torres, J. Martín-Pintado, S. Martín and M. R. Morris, *Astrophys. J.*, 2008, **672**, 352.
11 J. M. Lykke, A. Coutens, J. K. Jørgensen, M. H. D. van der Wiel, R. T. Garrod, H. S. P. Müller, P. Bjerkeli, T. L. Bourke, H. Calcutt, M. N. Drozdovskaya, C. Favre, E. C. Fayolle, S. K. Jacobsen, K. I. Öberg, M. V. Persson, E. F. van Dishoeck and S. F. Wampfler, *Astron. Astrophys.*, 2017, **597**, A53.
12 L. S. Bernstein and D. K. Lynch, *Astrophys. J.*, 2009, **704**, 226.
13 S. Albert, K. Keppler Albert, P. Lerch and M. Quack, *Faraday Discuss.*, 2011, **150**, 71.
14 S. Albert, Z. Chen, K. Keppler, P. Lerch, M. Quack, V. Schurig and O. Trapp, *Phys. Chem. Chem. Phys.*, 2019, **21**, 3669.
15 Z. Chen, S. Albert, K. Keppler, M. Quack, V. Schurig and O. Trapp, Proc. 2021 Int. Symposium on Molecular Spectroscopy, Urbana, IL, USA, paper WJ01, 2021, p. 182.
16 J. K. Jørgensen, M. H. D. van der Wiel, A. Coutens, J. M. Lykke, H. S. P. Müller, E. F. van Dishoeck, H. Calcutt, P. Bjerkeli, T. L. Bourke, M. N. Drozdovskaya, C. Favre, E. C. Fayolle, R. T. Garrod, S. K. Jacobsen, K. I. Öberg, M. V. Persson and S. F. Wampfler, *Astron. Astrophys.*, 2016, **595**, A117.
17 H. S. P. Müller, J. K. Jørgensen, J.-C. Guillemin, F. Lewen and S. Schlemmer, *Mon. Not. R. Astron. Soc.*, 2023, **518**(1), 185.
18 P. Jakobsen, P. Ferruit, C. Alves de Oliveira, S. Arribas, G. Bagnasco, R. Barho, T. L. Beck, S. Birkmann, T. Böker, A. J. Bunker, S. Charlot, P. de Jong, G. de Marchi, R. Ehrenwinkler, M. Falcolini, R. Fels, M. Franx, D. Franz, M. Funke, G. Giardino, X. Gnata, W. Holota, K. Honnen, P. L. Jensen, M. Jentsch, T. Johnson, D. Jollet, H. Karl, G. Kling, J. Köhler, M.-G. Kolm, N. Kumari, M. E. Lander, R. Lemke, M. López-Caniego, N. Lützgendorf, R. Maiolino, E. Manjavacas, A. Marston, M. Maschmann, R. Maurer, B. Messerschmidt, S. H. Moseley, P. Mosner, D. B. Mott, J. Muzerolle, N. Pirzkal, J.-F. Pittet, A. Plitzke, W. Posselt, B. Rapp, B. J. Rauscher, T. Rawle, H.-W. Rix, A. Rödel, P. Rumler, E. Sabbi, J.-C. Salvignol, T. Schmid, M. Sirianni, C. Smith, P. Strada, M. te Plate, J. Valenti, T. Wettemann, T. Wiehe, M. Wiesmayer, C. J. Willott, R. Wright, P. Zeidler and C. Zincke, *Astron. Astrophys.*, 2022, **661**, A80.
19 P. Ferruit, P. Jakobsen, G. Giardino, T. Rawle, C. Alves de Oliveira, S. Arribas, T. L. Beck, S. Birkmann, T. Böker, A. J. Bunker, S. Charlot, G. de Marchi, M. Franx, A. Henry, D. Karakla, S. A. Kassin, N. Kumari, M. López-Caniego, N. Lützgendorf, R. Maiolino, E. Manjavacas, A. Marston, S. H. Moseley, J. Muzerolle, N. Pirzkal, B. Rauscher, H.-W. Rix, E. Sabbi, M. Sirianni, M. te Plate, J. Valenti, C. J. Willott and P. Zeidler, *Astron. Astrophys.*, 2022, **661**, A81.
20 T. Böker, S. Arribas, N. Lützgendorf, C. Alves de Oliveira, T. L. Beck, S. Birkmann, A. J. Bunker, S. Charlot, G. de Marchi, P. Ferruit, G. Giardino, P. Jakobsen, N. Kumari, M. López-Caniego, R. Maiolino, E. Manjavacas, A. Marston, S. H. Moseley, J. Muzerolle, P. Ogle, N. Pirzkal, B. Rauscher, T. Rawle, H.-W. Rix, E. Sabbi, B. Sargent, M. Sirianni, M. te Plate, J. Valenti, C. J. Willott and P. Zeidler, *Astron. Astrophys.*, 2022, **661**, A82.
21 S. M. Birkmann, P. Ferruit, G. Giardino, L. D. Nielsen, A. García Muñoz, S. Kendrew, B. J. Rauscher, T. L. Beck, C. Keyes, J. A. Valenti, P. Jakobsen, B. Dorner, C. Alves de Oliveira, S. Arribas, T. Böker, A. J. Bunker, S. Charlot, G. de Marchi, N. Kumari, M. López-Caniego, N. Lützgendorf, R. Maiolino, E. Manjavacas, A. Marston, S. H. Moseley, N. Pirzkal, C. Proffitt, T. Rawle, H.-W. Rix, M. te Plate, E. Sabbi, M. Sirianni, C. J. Willott and P. Zeidler, *Astron. Astrophys.*, 2022, **661**, A83.
22 M. Quack, *Adv. Chem. Phys.*, 2014, **157**, 249.
23 A. Bacmann, A. Faure and J. Berteaud, *ACS Earth Space Chem.*, 2019, **3**(6), 1000.
24 B. E. Turner and A. J. Apponi, *Astrophys. J.*, 2001, **561**, L207.
25 H. E. Matthews, P. Friber and W. M. Irvine, *Astrophys. J.*, 1985, **290**, 609.
26 P. Coll, J.-M. Bernard, R. Navarro-González and F. Raulin, *Astrophys. J.*, 2003, **598**(1), 700.
27 C. Puzzarini, A. Baiardi, J. Bloino, V. Barone, T. E. Murphy, H. D. Drew and A. Ali, *Astrophys. J.*, 2017, **154**, 82.
28 C. Puzzarini, M. Biczysko, J. Bloino and V. Barone, *Astrophys. J.*, 2014, **785**, 107.
29 J.-M. Flaud, W. J. Lafferty, F. Kwabia Tchana, A. Perrin and X. Landsheere, *J. Mol. Spectrosc.*, 2012, **271**, 38.
30 C. Medcraft, C. D. Thompson, E. G. Robertson, D. R. T. Appadoo and D. McNaughton, *Astrophys. J.*, 2012, **753**, 1.
31 H. Hollenstein, D. Luckhaus, J. Pochert, M. Quack and G. Seyfang, *Angew. Chem., Int. Ed. Engl.*, 1997, **36**, 140.
32 R. A. Nyquist and W. Putzig, *Appl. Spectrosc.*, 1986, **40**, 112.
33 T. Nakanaga, *J. Chem. Phys.*, 1980, **73**, 5451.
34 T. Nakanaga, *J. Chem. Phys.*, 1981, **74**, 5384.
35 D. K. Russell and R. Wesendrup, *J. Mol. Spectrosc.*, 2003, **217**(1), 59.
36 R. A. Creswell and R. H. Schwendeman, *Chem. Phys. Lett.*, 1974, **27**, 521.

37 C. Hirose, *Astrophys. J.*, 1974, **189**, L145.
38 C. H. Townes and A. Schawlow, *Microwave Spectroscopy*, Dover, New York, 1975.
39 L. Pan, S. Albert, K. V. L. N. Sastry, E. Herbst and F. C. De Lucia, *Astrophys. J.*, 1998, **499**, 517.
40 F. Kwabia Tchana, J. M. Flaud, W. J. Lafferty and M. Ngom, *Mol. Phys.*, 2014, **112**, 1633.
41 M. Ngom, J.-M. Flaud, F. Kwabia-Tchana, W. J. Lafferty, X. Landsheere, A. Perrin and El. A. Ngom, *Can. J. Phys.*, 2013, **91**, 906.
42 W. J. Lafferty, J.-M. Flaud, F. Kwabia Tchana and J. M. Fernandez, *Mol. Phys.*, 2013, **111**, 1983.
43 C. Hirose, *Bull. Chem. Soc. Jpn.*, 1974, **47**(6), 1311.
44 H. S. P. Müller, J. K. Jørgensen, J.-C. Guillemin, F. Lewen and S. Schlemmer, *J. Mol. Spectrosc.*, 2023, **394**, 111777.
45 M. Suter and M. Quack, *Appl. Opt.*, 2015, **54**, 4417.
46 S. Albert, K. Albert Keppler and M. Quack, *Trends Opt. Photonics*, 2003, **84**, 177; S. Albert, K. Keppler, V. Boudon, P. Lerch and M. Quack, *J. Mol. Spectrosc.*, 2017, **337**, 105.
47 S. Albert, K. Keppler and M. Quack, High Resolution Fourier Transform Infrared Spectroscopy, in *Handbook of High-Resolution Spectroscopy*, ed. M. Quack and F. Merkt, Wiley, Chichester, 2011, vol. 2, pp. 965–1019.
48 F. Kwabia Tchana, M. Ngom, A. Perrin, J.-M. Flaud, W. J. Lafferty, S. A. Ndiaye and El. A. Ngom, *J. Mol. Spectrosc.*, 2013, **292**, 1.
49 S. Albert, Z. Chen, Ph Lerch, K. Keppler, M. Quack, V. Schurig and O. Trapp, in Proceedings of the XXth Symposium on Atomic, Cluster and Surface Physics (SASP2016), Davos, Switzerland, 7–12 February, Innsbruck University Press, Innsbruck, 2016, ISBN 078-903122-04-08, 2016, pp. 161–164.
50 S. Albert, Z. Chen, Ph Lerch, K. Keppler, M. Quack, V. Schurig and O. Trapp, 72nd International Symposium on Molecular Spectroscopy, Urbana, IL, USA, 17–21 June 2017, paper WA01, DOI: 10.15278/isms.2017.WA01.
51 K. K. Albert, S. Albert, M. Quack, J. Stohner, O. Trapp and V. Schurig, in Proceedings of the 19th Colloquium on High-Resolution Molecular Spectroscopy, Salamanca, Spain, 11–16 September 2005, Paper H15.
52 S. Albert, K. Keppler, C. Manca Tanner, M. Quack, Z. Chen, J. Stohner, P. Lerch, V. Schurig and O. Trapp, in proceedings of the 26th Colloquium on High-Resolution Molecular Spectroscopy, Dijon, France, 26–30 August 2019.
53 G. Guelachvili and K. Narahari Rao, *Handbook of Infrared Standards*, Academic Press, London, UK, 1986.
54 M. J. Frisch, G. W. Trucks, H. B. Schlegel, G. E. Scuseria, M. A. Robb, J. R. Cheeseman, G. Scalmani, V. Barone, G. A. Petersson, H. Nakatsuji, X. Li, M. Caricato, A. V. Marenich, J. Bloino, B. G. Janesko, R. Gomperts, B. Mennucci, H. P. Hratchian, J. V. Ortiz, A. F. Izmaylov, J. L. Sonnenberg, D. Williams-Young, F. Ding, F. Lipparini, F. Egidi, J. Goings, B. Peng, A. Petrone, T. Henderson, D. Ranasinghe, V. G. Zakrzewski, J. Gao, N. Rega, G. Zheng, W. Liang, M. Hada, M. Ehara, K. Toyota, R. Fukuda, J. Hasegawa, M. Ishida, T. Nakajima, Y. Honda, O. Kitao, H. Nakai, T. Vreven, K. Throssell, J. A. Montgomery, Jr., J. E. Peralta, F. Ogliaro, M. J. Bearpark, J. J. Heyd, E. N. Brothers, K. N. Kudin, V. N. Staroverov, T. A. Keith, R. Kobayashi, J. Normand, K. Raghavachari, A. P. Rendell, J. C. Burant, S. S. Iyengar, J. Tomasi, M. Cossi, J. M. Millam, M. Klene, C. Adamo, R. Cammi, J. W. Ochterski, R. L. Martin, K. Morokuma, O. Farkas, J. B. Foresman and D. J. Fox, *Gaussian 16, Revision C.01*, Gaussian, Inc., Wallingford CT, 2016.
55 C. M. A. Brett, J. G. Frey, R. Hinde, Y. Kuroda, R. Marquardt, F. Pavese, M. Quack, J. Stohner and A. J. Thor, *Quantities, Units and Symbols in Physical Chemistry, Abridged version*, IUPAC & Royal Society of Chemistry, Cambridge, 4th edn, 2023; E. R. Cohen, T. Cvitas, J. G. Frey, B. Holmström, K. Kuchitsu, R. Marquardt, I. Mills, F. Pavese, M. Quack, J. Stohner, H. L. Strauss, M. Takami and A. J. Thor, *Quantities, Units and Symbols in Physical Chemistry*, 3rd Printing, IUPAC & Royal Society of Chemistry, Cambridge, 3rd edn, 3rd Printing, 2011.
56 M. Quack and J. Stohner, *Chimia*, 2005, **59**, 530.
57 M. Quack, J. Stohner and M. Willeke, *Annu. Rev. Phys. Chem.*, 2008, **59**, 741.
58 M. Quack and J. Stohner, *Z. Phys. Chem.*, 2000, **214**, 675; M. Quack and J. Stohner, *Phys. Rev. Lett.*, 2000, **84**, 3807.
59 M. Quack and J. Stohner, *Chirality*, 2001, **13**, 745.
60 M. Quack and J. Stohner, *J. Chem. Phys.*, 2003, **119**, 11228.
61 J. Stohner, *Int. J. Mass Spectrom.*, 2004, **233**, 385.
62 J. K. G. Watson. in *Vibrational Spectra and Structure*, ed. J. R. Durig, Elsevier, Amsterdam, 1978, vol. 6, pp. 1–89.
63 S. Albert, K. Keppler Albert, H. Hollenstein, C. Manca Tanner and M. Quack, Fundamentals of Rotation–Vibration Spectra, in *Handbook of High-Resolution Spectroscopy*, ed. M. Quack and F. Merkt, Wiley, Chichester, 2011, vol. 1, pp. 117–173, LOOM4WANG was coded by Fabio Mariotti.
64 D. Luckhaus and M. Quack, *Mol. Phys.*, 1989, **68**(3), 745.
65 F. Merkt and M. Quack, Molecular Quantum Mechanics and Molecular Spectra, Molecular Symmetry, and Interaction of Matter with Radiation, in *Handbook of High-Resolution Spectroscopy*, ed. M. Quack and F. Merkt, Wiley, Chichester, 2011, vol. 1, pp. 1–55.
66 H. M. Pickett, *J. Mol. Spectrosc.*, 1991, **148**, 371.
67 C. M. Western, *J. Quant. Spectrosc. Radiat. Transfer*, 2017, **186**, 221; C. M. Western and B. E. Billinghurst, *Phys. Chem. Chem. Phys.*, 2019, **21**, 13986; C. M. Western and B. E. Billinghurst, *Phys. Chem. Chem. Phys.*, 2017, **19**, 10222; C. M. Western, Introduction to Modeling High-Resolution Spectra, in *Handbook of High-Resolution Spectroscopy*, ed. M. Quack and F. Merkt, Wiley, Chichester, 2011, vol. 1.
68 L. S. Rothman, I. E. Gordon, A. Barbe, D. Chris Benner, P. F. Bernath, M. Birk, V. Boudon, L. R. Brown, A. Campargue, J.-P. Champion, K. Chance, L. H. Coudert, V. Danaj, V. M. Devi, S. Fally, J.-M. Flaud, R. R. Gamache, A. Goldmann, D. Jacquemart, I. Kleiner, N. Lacome, W. J. Lafferty, J.-Y. Mandin, S. T. Massie, S. N. Mikhailenko, C. E. Miller, N. Moazzen-Ahmadi, O. V. Naumenko, A. V. Nikitin, J. Orphal, V. I. Perevalov, A. Perrin, A. Predoi-Cross, C. P. Rinsland, M. Rotger, M. Šimecková, M. A. H. Smith, K. Sung, S. A. Tashkun, J. Tennyson, R. A. Toth, A. C. Vandaele and

J. Vander Auwera, *J. Quant. Spectrosc. Radiat. Transfer*, 2009, **110**, 533.

69 I. E. Gordon, L. S. Rothman, R. J. Hargreaves, R. Hashemi, E. V. Karlovets, F. M. Skinner, E. K. Conway, C. Hill, R. V. Kochanov, Y. Tan, P. Wcisło, A. A. Finenko, K. Nelson, P. F. Bernath, M. Birk, V. Boudon, A. Campargue, K. V. Chance, A. Coustenis, B. J. Drouin, J.-M. Flaud, R. R. Gamache, J. T. Hodges, D. Jacquemart, E. J. Mlawer, A. V. Nikitin, V. I. Perevalov, M. Rotger, J. Tennyson, G. C. Toon, H. Tran, V. G. Tyuterev, E. M. Adkins, A. Baker, A. Barbe, E. Canè, A. G. Császár, A. Dudaryonok, O. Egorov, A. J. Fleisher, H. Fleurbaey, A. Foltynowicz, T. Furtenbacher, J. J. Harrison, J.-M. Hartmann, V.-M. Horneman, X. Huang, T. Karman, J. Karns, S. Kassi, I. Kleiner, V. Kofman, F. Kwabia-Tchana, N. N. Lavrentieva, T. J. Lee, D. A. Long, A. A. Lukashevskaya, O. M. Lyulin, V. Y. Makhnev, W. Matt, S. T. Massie, M. Melosso, S. N. Mikhailenko, D. Mondelain, H. S. P. Müller, O. V. Naumenko, A. Perrin, O. L. Polyansky, E. Raddaoui, P. L. Raston, Z. D. Reed, M. Rey, C. Richard, R. Tóbiás, I. Sadiek, D. W. Schwenke, E. Starikova, K. Sung, F. Tamassia, S. A. Tashkun, J. Vander Auwera, I. A. Vasilenko, A. A. Vigasin, G. L. Villanueva, B. Vispoel, G. Wagner, A. Yachmenev and S. N. Yurchenko, *J. Quant. Spectrosc. Radiat. Transfer*, 2022, **277**, 107949.

70 A. Bauder, Fundamentals of Rotational Spectroscopy, in *Handbook of High-Resolution Spectroscopy*, ed. M. Quack and F. Merkt, Wiley, Chichester, 2011, vol. 2, pp. 57–116.

71 G. Wichmann, G. Seyfang and M. Quack, *Mol. Phys.*, 2021, **119**(17–18), e1959073.

72 B. P. Winnewisser, J. Reinstädtler, K. M. T. Yamada and J. Behrend, *J. Mol. Spectrosc.*, 1989, **136**, 12. LW5.11 code: Fred Stroh.

73 S. Albert, M. Winnewisser and B. P. Winnewisser, *Ber. Bunsenges. Phys. Chem.*, 1996, **100**, 1876.

74 S. Albert, K. Albert Keppler and M. Quack, *J. Mol. Struct.*, 2004, **695–696**, 385.

75 S. Albert, H. Hollenstein, M. Quack and M. Willeke, *Mol. Phys.*, 2004, **102**, 1671.

76 F. Merkt and M. Quack, Molecular Quantum Mechanics and Molecular Spectra, Molecular Symmetry, and Interaction of Matter with Radiation, in *Handbook of High-Resolution Spectroscopy*, ed. M. Quack and F. Merkt, Wiley, Chichester, 2011, ch. 1, vol. 1, pp. 1–55.

77 M. Quack, *Bunsenmagazin*, 2022, **24**, 238.

78 J.-M. Flaud and J. Orphal, Spectroscopy of the Earth's Atmosphere, in *Handbook of High-Resolution Spectroscopy*, ed. M. Quack and F. Merkt, Wiley, Chichester, 2011, vol. 3, pp. 1971–1992.

79 L. M. Ziurys, Millimeter and Submillimeter Wave Spectroscopy and Astrophysical Applications, in *Handbook of High-Resolution Spectroscopy*, ed. M. Quack and F. Merkt, Wiley, Chichester, 2011, vol. 2, pp. 934–964.

80 Y. Ellinger, F. Pauzat, A. Markovits, A. Allaire and J.-C. Guillemin, *Astron. Astrophys.*, 2020, **633**, A49.

81 M. Quack, *Angew. Chem., Int. Ed.*, 2002, **41**, 4618.

82 R. Berger, M. Quack and J. Stohner, *Angew. Chem., Int. Ed.*, 2001, **40**, 1667.

83 M. Quack, *Chem. Phys. Lett.*, 1986, **132**(2), 147.

84 Y. Yamaguchi and H. F. Schaefer III, Analytic Derivative Methods in Molecular Electronic Structure Theory, A New Dimension to Quantum Chemistry and its Applications to Spectroscopy, in *Handbook of High-Resolution Spectroscopy*, ed. M. Quack and F. Merkt, Wiley, Chichester, 2011, vol. 1, pp. 325–362.

85 J. Tennyson, High Accuracy Rotation Vibration Calculations in Small Molecules, in *Handbook of High-Resolution Spectroscopy*, ed. M. Quack and F. Merkt, Wiley, Chichester, 2011, vol. 1, pp. 551–572.

86 T. Carrington, Using Iterative Methods to Compute Vibrational Spectra, in *Handbook of High-Resolution Spectroscopy*, ed. M. Quack and F. Merkt, Wiley, Chichester, 2011, vol. 1, pp. 573–586.

87 A. G. Császár, C. Fábri and T. Szidarovszky, Exact Numerical Methods for Stationary State Based Quantum Dynamics of Complex Polyatomic Molecules, in *Molecular Spectroscopy and Quantum Dynamics*, ed. R. Marquardt and M. Quack, Elsevier, 2021, ch. 2, pp. 43–78.

88 C. Fabri, R. Marquardt, A. G. Császár and M. Quack, *J. Chem. Phys.*, 2019, **150**, 01402.